ADVANCED FUNCTIONAL MATERIALS
www.afm-journal.de

Controllable Particle Adhesion with a Magnetically Actuated Synthetic Gecko Adhesive

Andrew G. Gillies, Jonghun Kwak, and Ronald S. Fearing*

Particle capture and release using controllable adhesion is of growing interest in many fields including reusable adhesives, solar panel cleaning, micromanipulation and robot locomotion where current methods of particle management are not sufficient. Here controllable adhesion to glass spheres with a new magnetically actuated synthetic gecko adhesive made from a magnetoelastomer composite is demonstrated. Adhesion is controlled by changing the effective elastic modulus of the surface through actuation of micro surface features with an external magnetic field. A compliant mechanics and magnetic torque analysis explains this general principle and generalizes the results for various geometries. Results show sphere pull-off forces can be increased 10-fold by changing the ridge orientation via the external magnetic field, and that the effective elastic modulus can be changed from 65 kPa to 1.5 MPa. Particle transport and release of 500- and 1000-micrometer glass spheres is also demonstrated.

1. Introduction

Particle capture and release is a significant problem in many industries such as in semiconductor manufacturing, solar panel cleaning and reusable adhesives for robot locomotion in complex and dirty environments.[1] Current methods of particle manipulation are insufficient for these applications where liquid solutions cannot be used, vibration or air jets are ineffective due to high surface area to volume ratios, and scrubbing is not an option due to delicate surfaces, geometric or environmental constraints.[2,3]

Recently, it has been shown that the adhesive structures found on the feet of geckos can shed particles after fouling in order to preserve the adhesive properties of the foot pads.[4] This 'dry self-cleaning' is explained by a change in the conformation of the nanofibrillar surfaces through passive mechanical action. These adhesive structures have inspired a new class of materials known as gecko-inspired synthetic adhesives (GSAs).[5] GSAs show several of the same remarkable behaviors as the gecko including directional adhesion, strong attachment with minimal preload, quick detachment, as well as dry self-cleaning under limited conditions.[6–8] While dry self-cleaning has been exhibited with GSAs, this effect has only been shown across a narrow range of particles and materials choices. As well, recent efforts have also gone into switchable adhesion by chemical functionality and topography, with some success by means of pH or temperature changes.[9] Switchable adhesion has been shown by Jeong et. al. in a nontransfering dry adhesive in transport of large smooth surface such as LCD screens, and Kim et al. created a microstructured elastic surface capable of transfer printing by modulating pressure on flat stiff objects.[10,11] To increase the versatility and effectiveness of GSA materials, and to improve self-cleaning capabilities, we studied active controllable adhesion with a new GSA across spherical particles.

The literature offers several examples of actively controlled fibrillar surfaces. Belardi created magnetic artificial cilia fabricated from photoreactive copolymer precursors filled with magnetic nanoparticles by a new photolithographic process.[12] The cilia are operated in a fluidic environment for micromixing, but particle adhesion to the array was not reported. Evans produced high aspect ratio nanorod arrays of a PDMS–ferrofluid composite material, and exhibited actuation for applications in photonics and sensing.[13] Northen fabricated a GSA on nickel cantilevers that, when actuated, decreased the adhesion of the structure to a glass flat punch.[14] However, to the authors' knowledge, no examples exist of a GSA showing controllable adhesion to particles for the purposes of particle capture and control. Here we report a new GSA made from a magnetoelastomer (ME) composite material actuated by an external magnetic field. The GSA is comprised of parallel microfabricated wedge-shaped microridges that are 100-μm wide at their base, and taper to less than 10-μm thick at their tips. The microridges are 325-μm long, and are formed in 15-mm-wide rows, 325 μm apart, similar to earlier work.[15]

ME composites are a new class of materials, generally involving a dispersion of carbonyl iron particles in a poly-dimethyl siloxane (PDMS) network.[16] Such materials have an elastic stiffness that can be tuned by an external magnetic field. To increase the magnetic reinforcement effect, the ME composite can also be cured under a magnetic field in order to align the carbonyl iron particles during curing.[17] Relevant examples of

A. G Gillies
Department of Mechanical Engineering
University of California
Berkeley, Berkeley, CA 94720, USA
E-mail: andrew.gillies@gmail.com
J. Kwak, Dr. R. S Fearing
Department of Electrical Engineering and Computer Science
University of California
Berkeley, Berkeley, CA 94720, USA

DOI: 10.1002/adfm.201203122

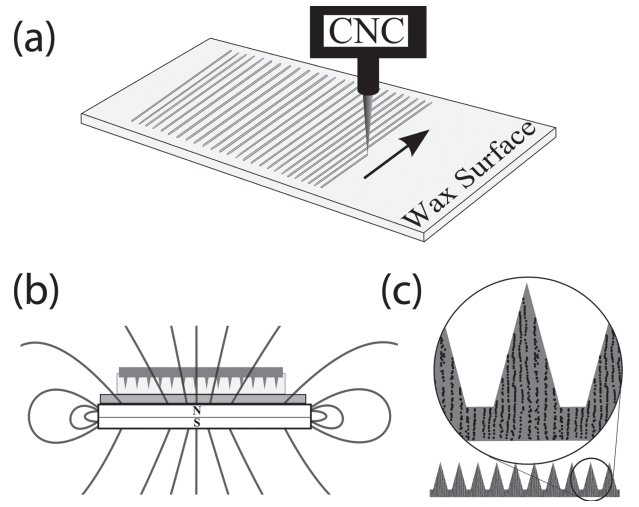

Figure 1. Fabrication of the magnetoelastomer microridges. a) A wax surface is inscribed with a custom-built 3 axis CNC machine. b) The magnetoelastomer material is cast into the wax mold, and allowed to cure in a magnetic field. c) While curing, the carbonyl iron particles align to form chains along the direction of the magnetic field.

devices that employ this material to effect a change in mechanical response include a microfluidic mixer capable of large deformations and a tunable elastic stiffness member capable of changes in elastic modulus of ~10×.[18,19]

2. Fabrication and Results

2.1. Fabrication

The microridges are fabricated by first forming a mold. The mold for the microridges is formed by cutting a wax plate with a pyramid cut tool guided by a custom-built 3 axis CNC machine.[15,20,21] Liquid PDMS (Mold Max 20, Smooth-On Inc.) is then mixed with carbonyl iron powder, with 6–9-μm grain size (≥99.5%, Sigma-Aldrich) in a 25% by weight ratio. The liquid elastomer mixture is then cast into the mold and degassed under vaccum for 10 min. The elastomer is then allowed to cure in the presence of a permanent magnet, 4 mm from the bottom surface, with a field strength of approximately 2000 Gauss (**Figure 1**). During curing, the carbonyl iron particles form into chains that are aligned with the magnetic field. The microridge array is demolded after curing for 24 h at room temperature. Cross sections of the resulting material reveal the alignment of the carbonyl iron particle chains with the magnetic field (**Figure 2**).

2.2. Results

Actuation of the array is tested by placing the material near a 2.5 × 2.5 × 1.25 cm nickel plated neodymium magnet (K&J Magnetics). Placing the magnet within 5 mm of the array causes the microridges to bend into alignment with the magnetic field, and as the magnet is moved away, the microridges return to their original vertical position (**Figure 3**). Using an online

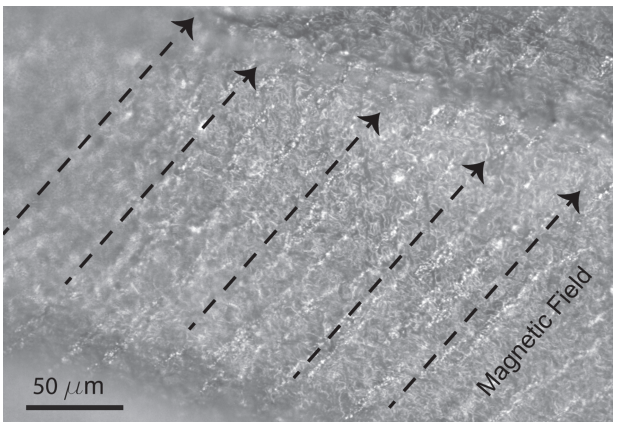

Figure 2. ME microridge, viewed from the side, showing chains of carbonyl iron particles (white), cured into alignment with a magnetic field (dashed black line).

magnetic field calculator (K&J Magnetics online field calculator, available at http://www.kjmagnetics.com/calculator.asp), the array deflection is plotted as a function of the magnetic field strength (**Figure 4**).

The effective elastic modulus of the array is determined experimentally using a sphere indenter test, and results show that the array has an effective elastic modulus of 65 kPa while

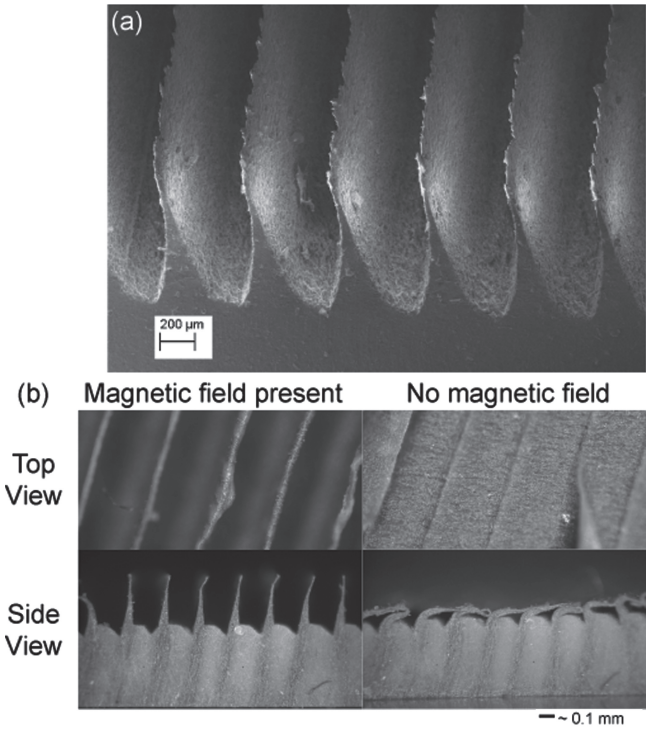

Figure 3. a) SEM of the completed magnetoelastomer microridges. The microridges are 325-μm long, 15-mm wide, and taper from 100 μm at their base to less than 10 μm at the tip. b) Actuation of the ridges, as seen from the top and side. In the presence of a magnetic field, the ridges completely flatten.

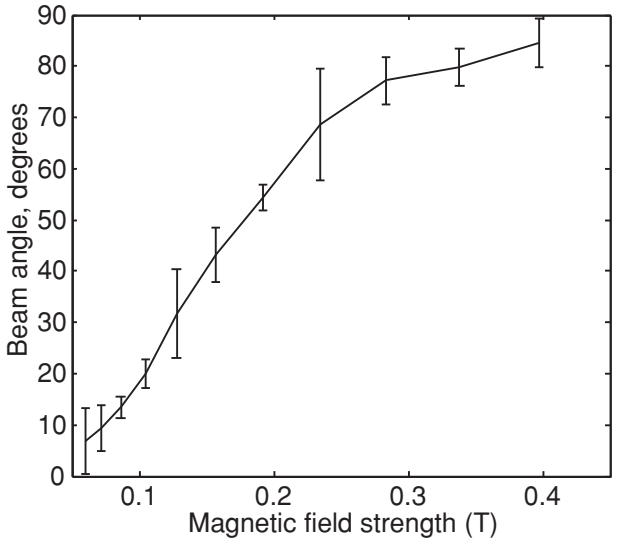

Figure 4. The microridge deflection from vertical as a function of the external magnetic field strength.

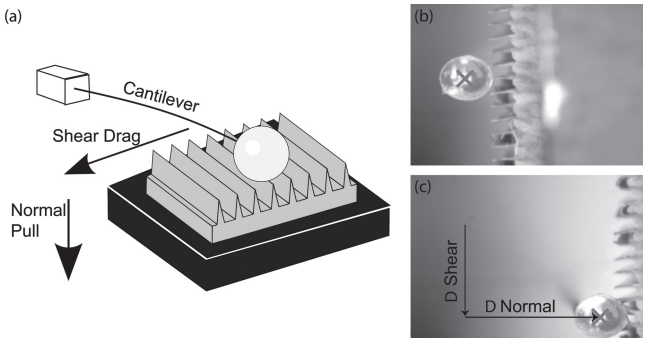

Figure 6. a) Schematic of the 2-axis wire cantilever apparatus used to test normal and shear adhesion between a glass sphere and the ME composite microridges. b,c) Images of a sphere adhering to the microridge array, showing normal and shear displacements. A video of test attached in the Supporting Information.

in the vertical orientation and 1.4 MPa in the flattened orientation at an indentation depth of 125 μm. **Figure 5** shows that vertical ridges are greater than 10 times more compliant at indentation depths of 125 μm, as compared to the flat actuated ridges, which at the same indentation level have effectively the same elastic modulus as a flat control surface.

Sphere adhesion to the array is tested by using a 2 axis cantilever wire with a glass sphere glued to the tip. By observing the deflection of the cantilever wire from above, we can infer the normal and shear adhesive forces on the sphere by Euler beam bending (**Figure 6**). Adhesion was tested on arrays in the vertical unactuated position and in the flattened actuated position with sphere probe sizes of 0.5 and 1 mm diameter. For the vertical position, results show that normal adhesion has a strong dependence on the shear load placed on the sphere (**Figure 7**). This effect, known as shear-induced normal adhesion, is a common feature of GSA's, and is used to control the normal adhesive strength by adjusting the shear loading on the array.[22] When the array is flattened in the presence of a magnetic field, the normal adhesion shows no dependence on the shear load, and the adhesion is ten times less than the vertical orientation. Adhesion tests on a smooth ME composite control sample confirm that the flattened ridges are effectively behaving like a smooth surface.

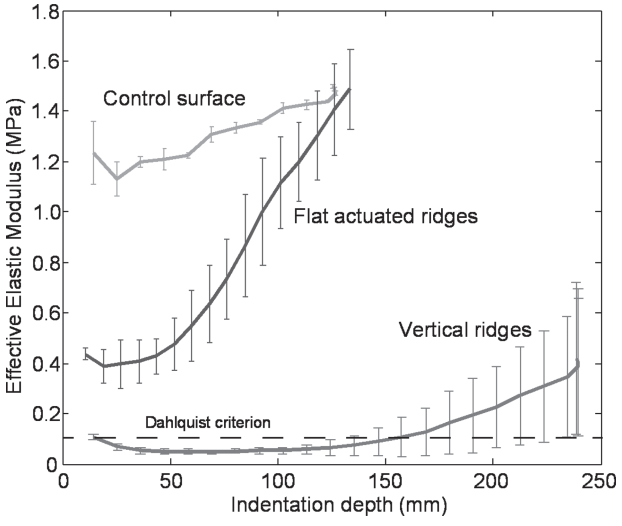

Figure 5. Results from a sphere indentation test show that vertical ridges are greater than 10 times more compliant at indentation depths of 125 μm, as compared to the flat actuated ridges, which at the same indentation level have the same compliance as a flat control surface (N = 3, error bars are ±1 s.d.). Vertical ridges also fall under the Dahlquist criterion for tack.

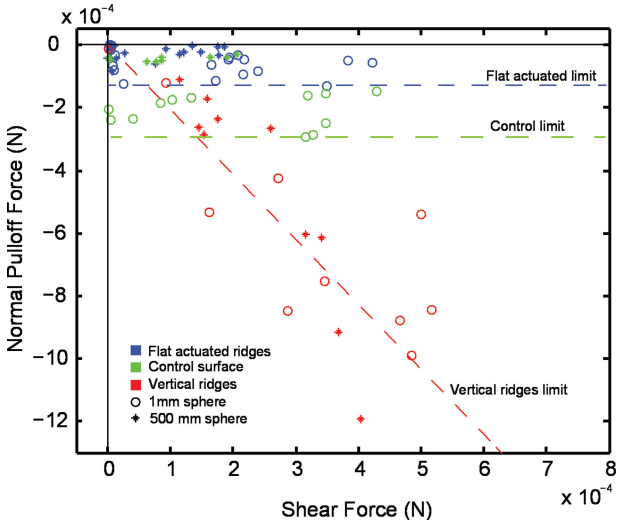

Figure 7. Data from sphere pull-off tests show that the microridge surface has a strong shear-induced normal adhesion effect while the ridges are vertical (red). Once ridges are activated and lie flat, the material acts the same as a smooth control sample and has ~10× less normal adhesion (blue). A smooth flat control surface (green) shows slightly larger adhesion than the flat actuated ridges. Open circles are 1mm spheres, asterisks are 500-μm spheres.

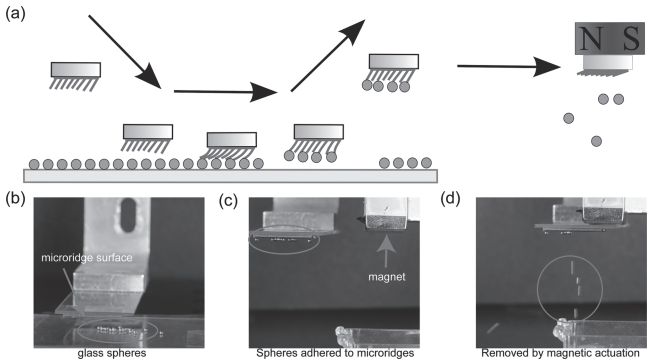

Figure 8. a) A proof-of-concept test in which the ME composite microridges are used to remove particles from a surface before being transported and actuated to release the particles into an adjacent hopper. b) Stills from video showing microridges, c) picking the particles off a surface, and then d) actuation of the microridges, causing particle detachment into the hopper. A video of the test is attached in the Supporting Information.

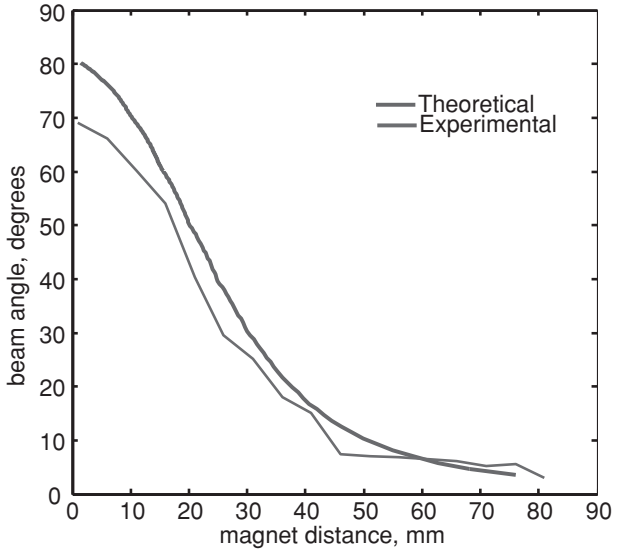

Figure 9. Theoretical analysis of beam angle has good agreement with a macroscale prototype of the ME composite microridges, and shows the beam angle dependence on the distance from a 2.5 cm × 2.5 cm × 1.25 cm neodymium magnet.

A proof of concept apparatus was also created to show how the material could be used for particle removal and release. Using a 3-axis displacement apparatus, the MR microridge material was brought into contact with glass slide covered with 500–1000-μm glass spheres. When sheared, the microridges adhere to the glass spheres, and the material is retracted. It is then moved to a permanent magnet. Once near the magnet, the microridges collapse flat, the adhesion with the spheres is lost, and the spheres fall into a hopper (**Figure 8**). A video of this test is available in the supplementary information, showing that nearly all the particles are transported from the glass surface into the hopper.

3. Discussion

To determine the magnetic field strength necessary to flatten the ridges, we solve for the equilibrium of torques acting on the beam.[23] We consider two torques, the elastic torque arising from the bending stiffness of the ridge, $T_{elastic}$, and the magnetic field torque, $T_{magnetic}$. Considering the large deflections observed, the elastic term is developed by considering the microridge as a rigid plate with a torsional spring at its base, with $T_{elastic} = K_{eq}\,\theta$. The equivalent stiffness of such a spring is found by (Equation 1):

$$K_{eq} = c_O \frac{E\,I}{l} \tag{1}$$

where E is the Young's modulus of the magnetoelastomer composite, I is an approximation of the second moment of area, l is the length of the microridge and c_o is a parametric angle coefficient.[24] A magnetic material, such as carbonyl iron, having magnetization (M), will experience a torque (T_m) in a magnetic field. This torque will rotate the magnetic moment into alignment with the magnetic field, and has strength found by (Equation 2):

$$T_{magnetic} = V_m\,\vec{M} \times \vec{H} \tag{2}$$

where V_m is the volume of the magnetic material, and H is the magnetic field strength.[24] The direction of the magnetization of the material is assumed to be along the length of the particle chains, parallel to the length of the ridges, while the strength of the magnetization is assumed to be at the saturation limit of carbonyl iron, 1.6 MA/m due to the presence of the strong magnetic field.[25] The resulting available torque from a misalignment between the external magnetic field and the ridge direction is found by (Equation 3):

$$T_{magnetic} = V_m \left|\vec{M}\right| \left|\vec{H}\right| \sin(\gamma - \theta) \tag{3}$$

Where γ is the angle of the fixed external magnetic field, and θ is the angle the ridge has deflected from its neutral position. Considering the ridge to be at equilibrium when $T_{magnetic} = T_{elastic}$ we get by (Equation 4):

$$\theta = \frac{V_m \left|\vec{M}\right| \left|\vec{H}\right|}{K_{eq}} \sin(\gamma - \theta) \tag{4}$$

This transcendental equation is solved numerically using Matlab. Ridge deflection, θ vs magnetic field strength is shown in **Figure 9**. A macroscale prototype consisting of nickel plates attached to a ground plate with a thin polymer flexure was created as a simple analog to verify the above analysis, since the actual microridges have nonlinear geometric properties that would require an analysis beyond the scope of this paper. The results show good agreement between the experiments on the macroscale prototype and the model (Figure 9).

A difference in the adhesive properties between the vertical and flattened positions can be explained by the change in effective stiffness between the two states. Previous studies have shown that below an elastic modulus of approximately 100 kPa, known as the Dahlquist criterion, the material surface becomes tacky.[26] A stiffer material, with a modulus well above the Dahlquist criterion can be made to have an effective modulus below 100 kPa through only the geometric design in

its surface. Considering the surface of the microridge material to be made of cantilever beams, we can calculate the change in effective stiffness between the vertical and flattened ridge position.[27,28] Assuming a sphere comes to rest between two ridges, we can approximate the ridges inclination angle, ϕ, to be 75°. Following Autumn's cantilever model,[27] we calculate the effective elastic modulus by (Equation 5):

$$E_{eff} = \frac{3 E I D \sin\varphi}{L^2 \cos\varphi^2} \quad (5)$$

Using the ridge dimensions as above, and taking the Young's modulus of the ME composite to be 1.5 MPa (determined by indentation experiments), we get an effective elastic modulus of ~35 kPa, well below the Dahlquist criterion.

This change in effective stiffness of the surface can be used in the Johnson Kendall Roberts (JKR) theory of contacting elastic solids to explain the change in adhesion between the two states. We use, as an approximation, the change in shear strength of the interface to predict the shear induced adhesion seen in Figure 7, and described Schubert et al.[7] and Tian et al.[30] For a rigid sphere on a flat elastic plane, the area of contact is related to the elastic modulus in JKR theory[29] by (Equation 6):

$$A_{JKR} \propto E^{-2/3} \quad (6)$$

Looking at the ratio of contact areas between the two cases, we get $\frac{A_{vertical}}{A_{flat}} \propto \left(\frac{E_{flat}}{E_{vertical}}\right)^{2/3}$ and from the measured values above, E_{vertical} = 75 kPa and E_{flat} = 1 MPa, we find an area ratio of 5.6 between the two cases. Assuming that the shear strength is proportional to the area of contact, $F_f \propto A_{JKR}$, we would expect to see a 5.6× increase in shear strength between the two cases, which is slightly less than the 10× increase we see in Figure 7.

Differences between the above model and the experimentally determined effective elastic modulus (Figure 5) of the array can be explained by nonlinearities arising from the complex shape of the ridges, as well as the large strains not considered in the model. However, the underlying principle remains intact, that being, in the vertical position, the ridges approximate a tacky surface. When the ridges are in the flat state, the effective elastic modulus approximates the bulk properties of the PDMS composite material, and the adhesion is lost. The surface now acts as if it had no microridge structures.

4. Conclusions

Particle capture and release using controllable adhesion is of interest in many fields including reusable adhesives, solar panel cleaning, micro-manipulation and robot locomotion where current methods of particle management are not sufficient. Here, we have demonstrated controllable adhesion to glass spheres with a new magnetically actuated synthetic gecko adhesive made from a magnetoelastomer composite. Capable of controlling adhesion to glass spheres 500 µm to 1 mm, this represents an important step in realizing an adhesive with dry self-cleaning capabilities across a wide range of particle sizes. Future work will involve integrating the microscale adhesive properties of this adhesive with the nanoscale adhesive properties of previously published results. This will make possible the next generation of reusable controllable adhesives that demonstrate dry self-cleaning across many orders of magnitude in particle size.

5. Experimental Section

Microridge Fabrication: Microridges are fabricated by first creating a wax mold. The mold is formed by melting paraffin wax on a glass slide at 80 °C, with a thickness of ~3 mm, and allowed to cool so that the top surface is smooth and uniform. The glass slide is then mounted into a custom-built 3 axis CNC machine, consisting of 3 microstepper stages (Zaber T-LSR150A) aligned with 2 two manual rotation stages (Newport RSP-2) and two linear slides with micrometers (Newport 423 slide) used for fine adjustment. The entire apparatus is mounted onto an air table (Newport VH series). The cutting tool (Bits and Bits, Profile Tool 10 degree 1/8" × 1-1/2") is mounted in the CNC chuck, and guided by the stages to cut 15 mm long slices in the wax that are 325 µm deep and have a row spacing of 325 µm. 125 rows are cut, giving a mold that is approximately 15 mm × 40 mm.

The magnetoelastomer composite is formed by first mixing the liquid PDMS base (Mold Max 20, Smooth-On Inc.) with carbonyl iron powder, 6–9 µm particle size, (≥99.5%, Sigma-Aldrich) in a 25% by weight ratio. Once the base and the carbonyl iron are thoroughly mixed by hand, the PDMS curing agent is added and thoroughly mixed. The mixture is cast into the wax mold and degassed in vacuum at 5 kPa abs for 10 min. After degassing, a second glass slide is placed over the liquid PDMS mixture, with a 400 g weight on top. This stack is then placed over a 5 cm × 5 cm × 0.635 cm Grade N42 Nickel Plated neodymium rare earth magnet (K&J Magnets). The weight prevents the magnetoelastomer from bulging in the magnetic field. The polymer is cured for 24 h before being removed from the mold.

Cantilever adhesion testing: Adhesion was tested using a 2-axis wire cantilever force sensor and an optical dissection microscope (Zeiss) connected to a computer via a digital camera (Paxcam). The cantilever, made from copper wire measuring 0.21 mm in diameter, had a glass sphere of varying size affixed to the tip via cyanoacrylate glue. The ME ridges were brought into contact with the glass sphere using two Newport linear slides with micrometers (Newport 423 slide). Deflections of the cantilever were recorded during the load-drag-pull tests using the software package Tracker (Tracker Video Analysis and Software Tool, Copyright (c) 2012 Douglas Brown). From the deflection measurements, adhesive forces can be calculated via Euler beam bending, where $F_{adh} = \frac{3EI\Delta}{l^3}$. Taking deflections in the normal and transverse directions is translated into normal and shear adhesion.

Effective Elastic Modulus Testing: The effective elastic modulus of the array was tested by using a sphere indentation apparatus similar to that described by Schubert.[7] A glass sphere indenter, with a radius of 20.3 mm was brought into contact with the array, under displacement control using a microstepper stage (Zaber T-LSR150A), while forces were recorded with a 6-axis force-torque sensor (Nano43, ATI Industrial Automation Inc.). Normal force measurements were used in conjunction with surface displacement measurements to determine the effective elastic modulus by the following equation[28]:

$$F_{normal} = \frac{4E_{eff}}{3(1-\nu^2)}\sqrt{R_p h^3}$$

where ν is the Poisson's ratio, taken here to be 0.5, R_p is the radius of the probe and h is the height of indentation from the neutral surface position. The results (Figure 5) show a low slope at the beginning of the indentation as the ridges bend over, and then a steepening of the curve as the ridges fully compress, and the backing begins to depress. From the above equation, an effective elastic modulus of 65 kPa is calculated for the vertical ridge surface, 1.4 MPa for the magnetically flattened surface, and 1.5 MPa for the control surface, at an indentation depth of 125 µm. 125 µm is used as the nominal indentation depth because

this is the approximate ridge penetration depth as observed in images of spheres on the array.

Macroscale Prototype and Model Confirmation: Due to the large nonlinearities and non-constant cross-section of the microridge profile, the approximate model was verified by using a simple macroscale prototype. The prototype consists of a nickel shim, 75-µm thick, cut into flaps measuring 15-mm wide and 2.5-mm long. The flaps are attached to the base via a polyethylene terephthalate flexure layer, 12-µm thick and 0.25-µm wide. The nickel flaps approximate nickel plates with hinges at their base, which have a stiffness approximated by $K_{eq} = \frac{EI}{l}$, where E, I and *l* are the polymer flexure modulus, second moment of inertia and length.[24] The deflection of the flaps is measured from horizontal in a magnetic field, and the strength of the magnetic field is controlled by placing a permanent magnet at varying distances from the flap in manner such that the orientation of the magnetic field is always vertical. Magnetic field strength is calculated using an online magnetic field strength calculator available at http://www.kjmagnetics.com/calculator.asp. Figure 9 shows good agreement between the model and the macroscale prototype.

Supporting Information

Supporting Information is available from the Wiley Online Library or from the author.

Acknowledgements

The authors thank the members of the Biomimetic Millisystems lab for their support. This work was funded by NSF grant 0856789.

Received: October 24, 2012
Revised: December 17, 2012
Published online: February 7, 2013

[1] L. Hecht, *J. IES* **1990**, *33*, 33.
[2] R. A Bowling, *Particles on Surface 1: Detection, Adhesion and Removal* (Ed: K. L. Mittal), Plenum. Press, New York, **1988**, p. 129
[3] K. Xu, R. Vos, G. Vereecke, G. Doumen, W. Fyen, P.W. Mertens, M.M. Heyns, C. Vinckier, J. Fransaer, *J. Vac. Sci. Technol., B* **2004**, *22*, 2844.
[4] W. R. Hansen, K. Autumn, *Proc. Natl. Acad. Sci. USA* **2005**, *102*, 385.
[5] M. K. Kwak, C. Pang, H.-E. Jeong, H.-N. Kim, H. Yoon, H.-S. Jung, K.-Y. Suh, *Adv. Funct. Mater.* **2011**, *21*, 3606.
[6] A. Parness, D. Soto, N. Esparza, N. Gravish, M. Wilkinson, K. Autumn, M. Cutkosky, *J. R. Soc. Interface* **2009,** *122*, 1223.
[7] B. Schubert, J. Lee, C. Majidi, R. S. Fearing, *J. R. Soc. Interface* **2008**, *5*, 845.
[8] J. Lee, R. S. Fearing, *Langmuir* **2008**, *24*, 10587.
[9] M. Kamperman, A. Synytska, *J. Mater. Chem.* **2012**. *22*, 19390.
[10] H. E. Jeong, J.-K. Lee, H. N. Kim, S. H. Moon, K. Y. Suh, *Proc. Natl. Acad. Sci. USA* **2009**, 106, 5639.
[11] S. Kim, J. Wu, A. Carlson, S. H. Jin, A. Kovalsky, P. Glass, Z. Liu, N. Ahmed, S. L. Elgan, W. Chen, P. M. Ferreira, M. Sitti, Y. Huang, J. A. Rogers, *Proc. Natl. Acad. Sci. USA* **2010**, *107*, 17095.
[12] J. Belardi, N. Schorr, O. Prucker, J. Rühe, *Adv. Funct. Mater.* **2011**, *21*, 3314.
[13] B. A. Evans, A. R. Shields, R. L. Carroll, S. Washburn, M. R. Falvo, R. Superfine, *Nano Lett.* **2007**, *7*, 1428.
[14] M. T. Northen, C. Greiner, E. Arzt, K. L. Turner, *Adv. Mater.* **2008**, *20*, 3905.
[15] E. W. Hawkes, E. V. Eason, A. T. Asbeck, M. R. Cutkosky, *IEEE/ASME Trans. Mechatronics* **2012**, *18*, 518.
[16] J. D. Carlson, M. R Jolly, *Mechatronics* **2000**, *10*, 15.
[17] Z. Varga, G. Filipcsei, M. Zrínyi, *Polymer* **2006**, *47*, 227.
[18] C. Majidi, R. J. Wood, *App. Phys. Let.* **2010**, *97*, 164104.
[19] J. Li, M. Zhang, L. Wang, W. Li, P. Sheng, W. Wen, *Microfluid. Nanofluid.* **2010**, *10*, 919.
[20] M. Sitti, *IEEE/ASME Adv. Intell. Mechatron.* **2003**, *2*, 886.
[21] A. G. Gillies, R. S. Fearing, *Langmuir* **2011**, *27*, 11278.
[22] K. Autumn, A. Dittmore, D. Santos, M. Spenko, M. Cutkosky, *J. Exp. Biol.* **2006**, *209*, 3569.
[23] J. W. Judy, R. S. Muller, H. H. Zappe, *J. Microelectromech. Syst.* **1995**, *4*, 162.
[24] L.L. Howell, *Compliant Mechanisms*, John Wiley & Sons, New York **2001**, p. 136.
[25] R. Adhikari, A. Sarkar, A. K. Das, *Rev. Sci. Instrum.* **2012**, *83, 013903*.
[26] C. A. Dahlquist, *Pressure-Sensitive Adhesives. In Treatise on Adhesion and Adhesives*, Vol. *2* (Ed: R. L. Patrick), Dekker, New York **1969**, p. 219.
[27] K. Autumn, C. Majidi, R. E. Groff, A. Dittmore, R. S. Fearing, *J. Exp. Biol.* **2006**, *209*, 3558.
[28] N. J. Glassmaker, T. Himeno, C.-Y. Hui, J. Kim, *J. R. Soc. Interface* **2004**, *1*, 23.
[29] K. Johnson, K. Kendall, A. Roberts, *Proc. R. Soc. London, Ser. A* **1971**, *324*, 301.
[30] Y. Tian, N. Pesika, H. Zeng, K. Rosenberg, B. Zhao, P. McGuiggan, K. Autumn, J. Israelachvili, *Proc. Natl. Acad. Sci. USA* **2006**, *103*, 19320.